PCCP

Physical Chemistry Chemical Physics

www.rsc.org/pccp

Volume 13 | Number 26 | 14 July 2011 | Pages 12101–12336

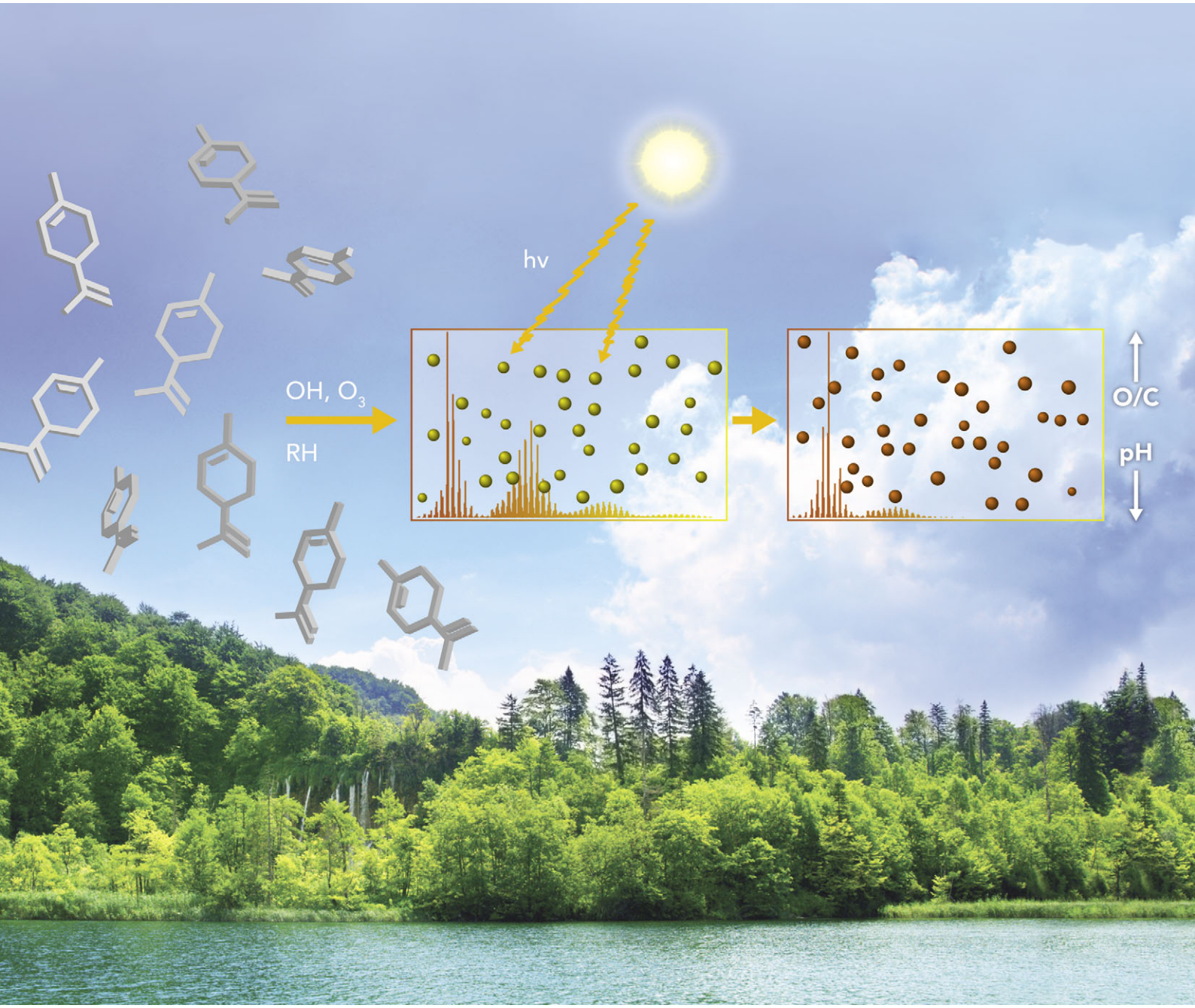

ISSN 1463-9076

COVER ARTICLE
Nizkorodov *et al.*
Photolytic processing of secondary organic aerosols dissolved in cloud droplets

HOT ARTICLE
Herrero *et al.*
Electrochemical and spectroscopic studies of ethanol oxidation on Pt stepped surfaces modified by tin adatoms

PCCP

Dynamic Article Links

Cite this: *Phys. Chem. Chem. Phys.*, 2011, **13**, 12199–12212

www.rsc.org/pccp

PAPER

Photolytic processing of secondary organic aerosols dissolved in cloud droplets†

Adam P. Bateman,[a] Sergey A. Nizkorodov,*[a] Julia Laskin[b] and Alexander Laskin[c]

Received 26th February 2011, Accepted 5th May 2011
DOI: 10.1039/c1cp20526a

The effect of UV irradiation on the molecular composition of aqueous extracts of secondary organic aerosol (SOA) was investigated. SOA was prepared by the dark reaction of ozone and d-limonene at 0.05–1 ppm precursor concentrations and collected with a particle-into-liquid sampler (PILS). The PILS extracts were photolyzed by 300–400 nm radiation for up to 24 h. Water-soluble SOA constituents were analyzed using high-resolution electrospray ionization mass spectrometry (HR-ESI-MS) at different stages of photolysis for all SOA precursor concentrations. Exposure to UV radiation increased the average O/C ratio and decreased the average double bond equivalent (DBE) of the dissolved SOA compounds. Oligomeric compounds were significantly decreased by photolysis relative to the monomeric compounds. Direct pH measurements showed that acidic compounds increased in abundance upon photolysis. Methanol reactivity analysis revealed significant photodissociation of molecules containing carbonyl groups and the formation of carboxylic acids. Aldehydes, such as limononaldehyde, were almost completely removed. The removal of carbonyls was further confirmed by the UV/Vis absorption spectroscopy of the SOA extracts where the absorbance in the carbonyl $n \rightarrow \pi^*$ band decreased significantly upon photolysis. The effective quantum yield (the number of carbonyls destroyed per photon absorbed) was estimated as $\sim$0.03. The total concentration of peroxides did not change significantly during photolysis as quantified with an iodometric test. Although organic peroxides were photolyzed, the likely end products of photolysis were smaller peroxides, including hydrogen peroxide, resulting in a no net change in the peroxide content. Photolysis of dry limonene SOA deposited on substrates was investigated in a separate set of experiments. The observed effects on the average O/C and DBE were similar to the aqueous photolysis, but the extent of chemical change was smaller in dry SOA. Our results suggest that biogenic SOA dissolved in cloud and fog droplets will undergo significant photolytic processing on a time scale of hours to days. This type of photolytic processing may account for the discrepancy between the higher values of O/C measured in the field experiments relative to the laboratory measurements on SOA in smog chambers. In addition, the direct photolysis of oligomeric compounds may be responsible for the scarcity of their observation in the field.

[a] *Department of Chemistry, University of California, Irvine, California 92617, USA. E-mail: nizkorod@uci.edu; Tel: +1-949-824-1262*
[b] *Chemical and Materials Sciences Division, Pacific Northwest National Laboratory, Richland, Washington 99352, USA*
[c] *Environmental Molecular Sciences Laboratory, Pacific Northwest National Laboratory, Richland, Washington 99352, USA*

† Electronic supplementary information (ESI) available: ESI (+) and ESI (−) mass spectra of SOA at different mass loadings (Fig. S1 and Fig. S2); ESI (+) mass spectra of photolyzed SOA extracts (Fig. S3); average values of O/C, H/C, DBE, OM : OC, and #C for all SOA mass loadings (Table S1); effect of dilution on the average values (Table S2); estimated fractions of carbonyls and carboxyls at different SOA loadings (Table S3); effect of photolysis on the fractions of carbonyls and carboxyls (Table S4); classification of compounds photolyzed on a filter by the effect of photolysis (Table S5). See DOI: 10.1039/c1cp20526a

Introduction

Biogenic emissions of volatile organic compounds (VOC) supply almost an order of magnitude more reduced carbon to the atmosphere than anthropogenic emissions.[1] Monoterpenes make up a significant fraction of these biogenic VOC emissions.[2] The ozone-initiated oxidation of monoterpenes results in formation of secondary organic aerosol (SOA) at high yields and is therefore an important contributor to the SOA budget.[3–5] Reaction of monoterpenes and ozone is also a major source of SOA in indoor environments.[6] SOA produced from the reaction of monoterpenes and ozone is a complex mixture of multi-functional organic compounds,[7,8] some of which may be detrimental to human health.[9]

Once produced, SOA can undergo photolytic processing in a dry state (particles containing small amounts of absorbed water), a wetted state (particles after significant hygroscopic growth), and a dissolved state inside cloud and fog droplets. After several days of such processing, the SOA material is removed from the atmosphere through wet and/or dry deposition and becomes part of terrestrial dissolved organic matter (DOM). Many properties of atmospheric water soluble organic carbon (WSOC) compounds are in fact similar to those of humic substances found in DOM from natural rivers and watersheds. Such WSOC compounds have been dubbed "humic like substances" or HULIS.[10]

Photolytic processing (direct UV irradiation) of dry biogenic SOA has been shown to involve direct photolysis of organic peroxides and carbonyl species.[11–13] Recent field observations also suggest significant photolytic processing of carbonyl compounds in aerosols during long range transport.[14] Biogenic SOA is sufficiently soluble to undergo moderate hygroscopic growth (growth factor about 1.1 at RH = 85%)[15] and nucleate clouds.[16–19] Indeed, WSOC compounds are ubiquitous in atmospheric rainwater samples[20–26] and in suspended cloud/fog droplets.[27–40] Dissolved in droplets, the SOA constituents become accessible to aqueous photolytic processing, which may be quite different from that occurring in dry particles.[41,42] Photolytic processing of field-collected SOA, DOM, and model organic compounds in aqueous solution has been investigated in a number of studies.[43–53] Aqueous OH radical initiated oxidation of organics, referred to as photochemical processing in recent literature, has also been investigated.[54–58] In photochemical processing experiments, H_2O_2 is intentionally added to the solution as an OH precursor, whereas in photolytic processing, the solution is photolyzed directly without any additions. These two types of processing are closely related because H_2O_2 is itself a product of photolysis of aqueous solutions of organics.[43,51,59,60]

This paper examines photolytic processing of aqueous solutions of SOA generated by oxidation of d-limonene, one of the six most common monoterpenes.[2] The chemical composition of d-limonene SOA has been extensively studied and a number of compound classes have been identified, making it an ideal model system for this work.[7,8,61–70] Although we have chosen a specific type of SOA for our experiments, we believe that our findings are not limited to d-limonene SOA but can be generalized to most types of biogenic SOA.

Due to the complexity and wide variability of SOA and DOM constituents, sophisticated analysis tools are required for their detailed chemical characterization. High-resolution mass spectrometry (HR-MS) has recently emerged as a powerful technique for studying laboratory generated organic aerosol,[7,8,69–72] biomass burning aerosol,[73,74] field-collected aerosol,[75–77] and DOM from a variety of sources.[20,28,49,50,78–82] This work takes full advantage of HR-MS methods to characterize transformations of SOA constituents upon exposure to UV radiation in both dry and aqueous conditions. Previously a number of laboratory studies focused on aqueous photochemistry of individual organic compounds.[52,53,44,45] The photochemistry of aqueous solutions of biogenic SOA, however, has not been studied in detail. In this work, we investigate the photochemistry of a complex mixture of organics that more closely approximates biogenic aerosol in the atmosphere. This type of holistic approach reveals important new aspects of aqueous photolytic processing of SOA. The HR-MS results presented here clearly demonstrate that the organic molecules associated with biogenic SOA undergo significant photolytic processing between the formation and removal of the particles in the atmosphere.

Experimental

Particle generation and collection

The dark reaction of d-limonene (Acros Organics, 98% purity) vapor and ozone was used to generate SOA (referred to as "limonene SOA" henceforth) in a 5 m^3 inflatable Teflon chamber.[72] The chamber was filled with dry filtered air generated from a purge-gas generator (Parker Balston, Model 75-62). Ozone was added by passing ultra-high purity oxygen (99.994%) through a Teflon tube with inserted Hg pen-ray UV lamp (Jelight Company, Inc.), until the mixing ratio stabilized at a desired level (0.05–1 ppm). The ozone concentration was measured with a photometric ozone analyzer (Thermo Scientific, Inc., Model 49i). Liquid d-limonene was injected into a small glass bulb with a microsyringe through a gas-tight septum and quantitatively transferred into the chamber with a flow of dry purified air. The amount of d-limonene was selected such that its mixing ratio in the chamber was approximately equal to that of ozone (1 : 1 stoichiometry). Multiple sets of experiments were performed with the initial mixing ratios of limonene and ozone equal to 1, 0.5, 0.1 and 0.05 ppm. No scavenger for hydroxyl radicals was added. The SOA examined in this work is likely a mixture of OH and ozone oxidation products of limonene as the yield of OH radical from limonene ozonolysis has been estimated at $\sim$80%.[83] Furthermore, because the oxidant is not present in excess, some of the products may still contain unreacted C=C bonds. The chamber air was mixed with a fan for $\sim$5 min after the injection of limonene. The fan was then turned off to minimize particle losses on the chamber walls. Particle concentrations were measured throughout the experiments with a scanning mobility particle sizer (SMPS, TSI Model 3080), consisting of a differential mobility analyzer (TSI Model 3081) and condensation particle counter (TSI Model 3775). Particles were detected within $\sim$5 min of the limonene injection under all reaction conditions. The SOA mixture remained inside the chamber, in the dark, for one hour prior to particle collection. Relative humidity in the chamber was below 2%.

A particle-into-liquid sampler (PILS)[84] (Brechtel Manufacturing, Inc.) was used to collect aqueous extracts of SOA. The PILS mixes saturated water vapor with the aerosol sample flow to grow the particles into larger droplets. The droplets are then impacted onto a vertical surface with a constant flow of flush water which is directed into 2 mL brown glass vials. The PILS inlet flow was fixed at 14 SLM, while the collection time and the flow of flush water varied depending on initial precursor concentration as summarized in Table 1. Under the present experimental conditions, the collected SOA material is expected to be fully dissolved in water. The vials with the collected samples were then frozen, pending later photolysis

Table 1 Initial conditions and reaction parameters for the SOA preparation (measured and/or calculated from the SMPS data). The quoted uncertainties represent one standard deviation from averaging results of repeated experiments

Initial concentrations (Ozone = Limonene)	PILS vial collection time (min)[a,b]	PILS water flow rate (μL/min)[b]	SOA mass concentration at the start of collection[c] (μg/m^3)
1 ppm	10 or 15	100	5300 ± 1000
0.5 ppm	10 or 15	100	1800 ± 300
0.1 ppm	20 or 30	50	290 ± 60
0.05 ppm	30 or 45	33	100 ± 30

[a] The particle collection started 1 h after mixing ozone and limonene. [b] Each of the PILS vials contained 1 or 1.5 mL at the end of the collection. [c] Mass concentration calculated from SMPS data assuming particle density of 1.2 g/cm^3.

experiments or mass spectrometric analysis. In selected experiments, additional samples were collected on a Fluoropore PTFE 0.22 μm filter (Millipore) at the same sampling flow rate of 14 SLM.

Photolysis of aqueous and dry SOA samples

The PILS samples were thawed and transferred into a standard 1 cm quartz cuvette where they were irradiated for up to 24 h in open air. The samples were exposed to lab air during photolysis and therefore contained dissolved oxygen. The radiation from a 100 W Xenon lamp placed in a Newport Photomax housing was reflected by a 90-degree 330 nm dichroic mirror, filtered with a 295 nm high-pass filter (Schott WG-295), and further filtered with a 2.5 cm cell containing water (to reduce sample heating by residual near-IR radiation), before entering the cuvette. The water temperature in the photolysis cell typically stabilized at 1–2 degrees C above room temperature. The total radiation power incident on the sample was ~1 W, as measured using a power meter (Coherent FieldMate, Model PS19Q). The wavelengths were confined to 300–400 nm as measured using a portable UV/Vis spectrometer (Ocean Optics, Model USB4000). UV/Vis spectra were obtained before and after photolysis using a dual-beam UV/Vis spectrometer (Shimadzu, Model UV-2450) with nanopure water as the reference. The samples were then transferred into clean 2 mL storage vials and frozen again for later mass spectrometric analysis or pH and peroxide content tests.

Photolysis experiments for dry SOA were conducted directly on filters. The filters were cut in half, with one half saved as a reference and the other half irradiated in the same setup as used for the aqueous photolysis. The filters remained in open air during photolysis. After irradiation, the filters were stored frozen in sealed containers and in the dark, until analysis.

Peroxide concentration and pH measurements

The collection times for the PILS samples were increased to collect 1.5 mL (the full vial capacity) of SOA aqueous extracts. The vial content was then divided into two 0.75 mL aliquots. One sample was photolyzed using the system described above, while the other was kept in the dark. The photolyzed and reference samples were mixed with 0.75 mL of nanopure water and transferred into separate 5 mL conical vials. The pH was measured using a Mettler Toledo SevenEasy™ S20 pH meter with InLab^R surface electrode. The dilution with water was necessary to allow the solution to come into full contact with the electrode surface.

Following the pH measurements, a peroxide test was performed on each sample as described by Nguyen *et al.*[72] (a modified procedure of Docherty *et al.*[85]). The solutions were acidified with 0.75 mL glacial acetic acid (EMD, 99.7% purity). After ~5 min of purging with N_2 (g), 0.25 mL of a 0.7 M potassium iodide solution was added and allowed to react for 1 h with constant mixing under a nitrogen atmosphere. The UV/Vis absorbance was measured at 470 nm in 1 cm quartz cells. The peroxide test was calibrated against diluted H_2O_2 (Fisher, ACS certified at 3.1%) measured under identical conditions.

Mass spectrometry

Immediately prior to the HR-MS analysis, the aqueous samples were thawed and 0.5 mL of each sample was mixed with 0.5 mL of acetonitrile. The filter halves were brought to room temperature, extracted in 0.75 mL water under sonication and then mixed with 0.75 mL acetonitrile. The addition of acetonitrile decreases the surface tension of the solution and facilitates a stable electrospray ionization process.[78] Mass spectra were recorded with a Finnigan LTQ (linear ion trap)-Orbitrap hybrid mass spectrometer (Thermo Electron Corporation, Inc.) with a modified ESI (electrospray ionization) source. The sample solutions were injected at a flow rate of 1.0 μL min^{-1} through a pulled fused silica capillary (50 μm i.d.). The instrument was operated with a mass resolving power of $m/\Delta m$ = 60 000 at m/z 400 in both positive and negative ionization modes. Mass calibration was performed using a standard calibration mix MSCAL 5 (Sigma-Aldrich, Inc.).

A typical set of HR-MS measurements included a series of SOA aqueous extracts or filter samples photolyzed for different times and reference (non photolyzed) samples. Blank samples included acetonitrile/water mixture and photolyzed nanopure water diluted with acetonitrile after the photolysis. In the case of filter experiments, blank samples represented photolyzed clean filters that were extracted with water and further diluted with acetonitrile in the same way as for the SOA-loaded filters.

All mass spectra from the same set of experiments were aligned to a common m/z axis, for each ionization mode. Background peaks present only in the blank samples were removed from all spectra. Peaks that were present in both sample and background spectra were retained if they were more intense in the former by a factor of 3 and larger. Molecular formulae were assigned based on accurate mass measurements, with restrictions imposed on the atom valence states and atomic ratios.[86] The observed ionization

mechanisms were Na^+ addition or protonation in the (+) mode, and deprotonation in the (−) mode. The molecular weights of the SOA compounds were then calculated from the m/z of the corresponding molecular ions. All data discussed in this study corresponds to the neutral SOA constituents in order to facilitate comparison between the (+) and (−) mass spectra.

The double bond equivalent (DBE)[87,88] value was calculated for each neutral SOA species. The DBE value is equal to the total number of double bonds (C=C and C=O), and rings in a $C_cO_oH_h$ molecule, and is calculated as:

$$\mathrm{DBE} = 1 - \frac{h}{2} + c \quad (1)$$

O/C and H/C ratios were calculated from the compounds' molecular formulas. The *average* DBE values, O/C ratios, H/C ratios, and the organic mass (OM) to organic carbon (OC) ratio were calculated from all assigned peaks in a given mass spectrum as follows:

$$\langle \mathrm{DBE} \rangle = \sum_i x_i \mathrm{DBE} \Big/ \sum_i x_i \quad (2)$$

$$\langle \mathrm{O/C} \rangle = \sum_i x_i o_i \Big/ \sum_i x_i c_i \quad (3)$$

$$\langle \mathrm{H/C} \rangle = \sum_i x_i h_i \Big/ \sum_i x_i c_i \quad (4)$$

$$\langle \mathrm{OM/OC} \rangle = 1 + \frac{16}{12}\langle \mathrm{O/C} \rangle + \frac{1}{12}\langle \mathrm{H/C} \rangle \quad (5)$$

where x_i correspond to the observed ion peak abundances. In the following text, the notation "average X" and "⟨X⟩" is used interchangeably.

It is well known that ESI mass spectral abundances are influenced by the solution composition, concentration of analytes and instrumental factors.[89,90] Previous research has indicated that surface active molecules with a significant non-polar carbon skeleton and an ionizable functional group are most responsive to ESI.[89,91] As most limonene oxidation products retain part of their hydrocarbon backbone and contain at least one polar functional group, they should have significant surface activities and comparable sensitivities to ESI. However, compounds such as aliphatic hydrocarbons, polycyclic aromatic hydrocarbons and/or cholesterol, will not be observed in the ESI spectrum. Even though it is rather unlikely that such non-polar compounds will be formed in limonene oxidation, it must be stressed that average quantities calculated in this paper are *not absolute* as they are derived from the ESI mass spectra. We note that, in the case of limonene SOA, the values calculated from eqn (2)–(5) are not strongly dependent on the specific choice of x_i; setting all of the x_i to 1 produces almost the same results as using relative peak intensities as weights.[69] This gives us confidence that the numbers obtained from eqn (2)–(5) are not too different from the true values.

Methanol reactivity analysis was employed to identify selected functional groups in SOA constituents, as has been previously described.[7] Briefly, SOA was collected onto filters and cut into quarters. Each quarter was dissolved in a different solvent, methanol, d_3-methanol, acetonitrile and d_3-acetonitrile. The presence of carbonyl functional groups was determined by observation of new/increased hemiacetal peaks corresponding to $\Delta(m/z)$ values of 32.0262 ($+CH_3OH$) and 35.0450 ($+CD_3OH$) for methanol and d_3-methanol, respectively. The presence of carboxyl functional groups was determined by observation of new/increased ester peaks corresponding to $\Delta(m/z)$ values of 14.0156 ($+CH_3OH–H_2O$) and 17.0345 ($+CD_3OH–H_2O$) for methanol and d_3-methanol, respectively. The addition of d_3-methanol to a carbonyl and esterification of carboxylic acids result in unique, easily identifiable peaks and were used to distinguish carbonyl and carboxyl groups. Multifunctional compounds could be detected by the observation of both the hemiacetal peak and ester peak detected at the exact mass corresponding to either methanol or d_3-methanol addition. Carbonyl compounds could be further classified as either aldehydes or ketones depending on the observed extent of their reaction with methanol. It was previously found that ~42% (by number) of ESI-MS detectable limonene SOA compounds with MW 100–500 Da contain at least one carbonyl group and ~55% contain at least one carboxyl group.[7] In this work, we have relied on the methanol reactivity to separate the SOA compounds into four classes, where molecules in each class contain: (1) at least one carbonyl group, (2) at least one carboxyl group, (3) both a carbonyl and a carboxyl group, and (4) other compounds with no carbonyl and carboxyl groups. These four classes of compounds were examined by HR-MS at different SOA precursor concentrations and photolysis times. We note that this classification was based on the compounds that were initially present in the 1 ppm SOA sample. Therefore, any new compounds appearing in mass spectra of photolyzed SOA and in mass spectra of samples with lower precursor concentration had to be placed in the "other functional group" category even though they could still contain carbonyl or carboxyl functional groups.

Results

Composition of limonene SOA prior to the photolysis

Chamber experiments on organic aerosols are typically done at elevated reactant concentrations in order to achieve sufficient sensitivity and avoid interference from impurities in the chamber. While the ozone concentrations used to prepare limonene SOA (0.05 to 1 ppm) overlap with the atmospherically relevant values, the limonene concentrations are 1–2 orders of magnitude higher than typical ambient values. The particle mass loading (calculated from the SMPS data) resulting from SOA precursor concentrations of 0.05 to 1 ppm were 100 to 5300 $\mu g/m^3$ (Table 1). The corresponding concentrations of dissolved SOA in the PILS samples ranged from 16 to 400 μg/mL, or from 80 μM to 2 mM, assuming an effective molecular weight of 200 g/mol for SOA compounds and a particle density of 1.2 g/cm^3.[92] The concentrations used in this study are of the same order of magnitude as concentrations of organics observed in cloud water (micro to millimolar).[93,94] Liquid water content of wetted aerosol particles is typically 3–5 orders of magnitude smaller than that of cloud/fog

droplets, resulting in concentrations of dissolved organics on the order of 0.1–10 M.[95] Therefore the present experimental conditions are more relevant for cloud/fog droplets than for wetted aerosols.

The ESI mass spectra were similar in appearance to those published previously.[7,8] Figure S1 and S2 of the supporting information (SI)† section contain representative (+) and (−) mass spectra collected at all precursor concentrations prior to photolysis. The overall shape of the limonene SOA mass spectra did not change significantly as the precursor concentration was reduced. For example, the relative intensity of the dimer peaks (300–500 amu) with respect to the monomer peaks (100–300 amu) was approximately the same at all concentrations. The relative intensities of the trimer and tetramer decreased somewhat at the lower SOA loadings.

Useful information can be gained from various average quantities such as elemental ratios, OM/OC values, DBE values, and number of carbon atoms per molecule (#C) calculated from the entire set of observed limonene SOA compounds.[69] These values are tabulated in Table S1 of the SI section.† The average O/C and DBE values are also plotted *versus* the concentration of SOA precursors in Fig. 1. The ⟨O/C⟩ values calculated from the ESI (−) spectra are systematically larger. At 1 ppm ozone and limonene, the calculated ⟨O/C⟩ are 0.40 and 0.50 in the (+) and (−) ionization modes, respectively, and agree well with previously published values of 0.43 and 0.50 for SOA generated at 10-times higher precursor concentration.[8] Systematically higher ⟨O/C⟩ values derived from the ESI (−) mass spectra are attributed to the preferential detection of more oxygenated compounds in the ESI (−) mode. The increase in ⟨DBE⟩ with the SOA precursor concentrations reflects the increase in high-MW oligomeric compounds, which tend to have large DBE values (Fig. S1 and S2 of the SI section).†[69] The increase in the relative abundance of the high-MW oligomeric compounds with SOA precursor concentration can also be observed from the increase in ⟨#C⟩.

The differences described above could reflect different chemical composition of SOA with different chamber loadings or the response of ESI mass spectra to the effects of dilution. In order to assess the effect of dilution, the same stock solution of limonene SOA was diluted a number of times, up to 1000 : 1 dilution factor, and an ESI mass spectrum was recorded and analyzed for each dilution level. Average values were calculated for each mass spectrum generated and tabulated in Table S2 of the SI section.† No significant changes to ⟨O/C⟩, ⟨H/C⟩, or ⟨OM : OC⟩ were observed from the dilution experiments. However, the ⟨DBE⟩ and ⟨#C⟩ values decreased somewhat at lower concentrations. Although it is difficult to completely decouple the effect of dilution from the real change in chemical composition with SOA chamber loading, the former appears to be modest relative to the latter. We would like to emphasize that for a given concentration, the photolysis induced changes in the average properties can be meaningfully compared as long as photolysis does not result in a significant depletion of organics from solution by evaporation of smaller products.

An interesting trend in Fig. 1 is the small but reproducible increase in ⟨O/C⟩ as the precursor concentration and the resulting SOA mass loading decreases (this change in ⟨O/C⟩ is not observed in the dilution experiments, and must therefore correspond to an actual change in SOA chemical composition). The ⟨O/C⟩ value increased from 0.40 to 0.43 and 0.50 to 0.53 in the ESI (+) and (−) modes, respectively, when the precursor concentrations decreased from 1 ppm to 0.05 ppm (the corresponding SOA mass loadings changed from ~5300 μg/m^3 to 100 μg/m^3). An increasing degree of oxidation at lower mass loadings was also reported for α-pinene SOA.[96,97] This effect likely arises from a change in the gas-to-particle partitioning of semivolatiles. At high OM concentrations in the chamber, less oxygenated compounds with low O/C can partition effectively into the particle phase, whereas the same compounds partition predominantly into the gas-phase at lower OM concentrations.

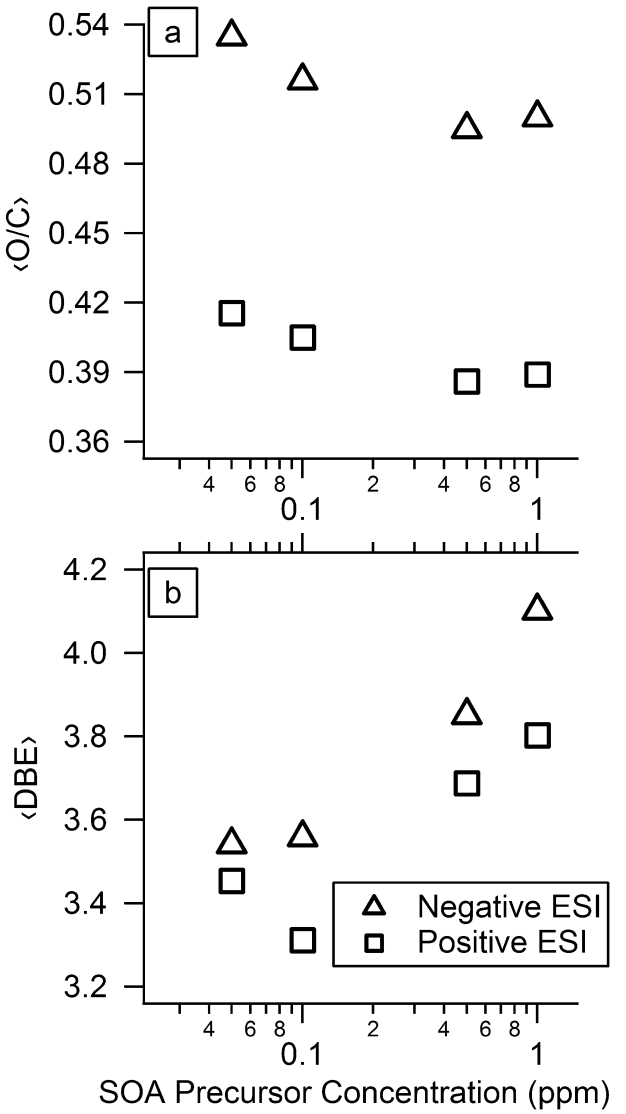

Fig. 1 Average O/C and DBE values of SOA constituents before photolysis derived from ESI (+) and ESI (−) mass spectra of PILS samples and plotted against the initial d-limonene concentrations used for the SOA generation (Table 1).

The partitioning was further examined by tracking the subsets of carbonyl and carboxyl peaks determined using methanol reactivity.[7] Table S3 in the SI section† details the percent of total abundance from compounds with carbonyl functional groups, carboxyl functional groups, both carbonyl

and carboxyl groups, and compounds with other functional groups, for all SOA precursor concentrations in both (+) and (−) ESI modes. The fraction of detected carboxylic acids increases with decreasing SOA mass loading, from ~8 to 13% and from 14 to 21% in the negative and positive ionization modes, respectively. This reflects the lower vapor pressures of carboxylic acids relative to carbonyls or alcohols of the same size.

Effect of photolysis on the HR-ESI-MS spectra of limonene SOA in water

Fig. 2 displays ESI (−) mass spectra acquired from the samples of (a) 1 ppm limonene SOA before photolysis, (b) after 2 h, and (c) 24 h of photolysis (Fig. S3 of the SI section† contains the corresponding ESI (+) mass spectra). Photolysis results in significant changes to the relative abundances of SOA peaks. For example, the trimeric and tetrameric compounds present in the initial sample (Fig. 2a) are almost fully degraded after 24 h of photolysis (Fig. 2c). Photodegradation of oligomeric species has also been observed during photochemical processing of dissolved organics with OH radical.[58]

The average elemental ratios and DBE values, before and after photolysis, are listed in Table S1 in the SI section,† for all experimental conditions. UV photolysis has no significant effect on ⟨H/C⟩ but it tends to increase ⟨O/C⟩, decrease ⟨DBE⟩, increase ⟨OM/OC⟩, and decrease ⟨#C⟩. Fig. 3 shows the ⟨O/C⟩ and ⟨DBE⟩ values for all UV irradiation times plotted as a function of the SOA precursor concentrations. Although the UV irradiation increases ⟨O/C⟩ at all concentrations, the most significant change occurs at higher concentrations (Fig. 3a). A possible explanation for this concentration effect is an increased fraction of photochemically active carbonyls in particles at higher mass loadings, and conversely an increased fraction of photochemically inactive carboxylic acids at lower mass loadings. This hypothesis is supported by the significant increase in the fraction of carbonyl and carbonyl/carboxyl containing compounds at high mass loading inferred from the methanol reactivity (Table S3 in the SI section†).

The decrease in ⟨DBE⟩ upon photolysis is observed at all precursor concentrations (Fig. 3b). This decrease can be attributed to the preferential photolytic dissociation of high-MW oligomeric compounds, as seen in the mass spectra shown in Fig. 2. As the average DBE values for monomers, dimers, trimers, and tetramers are ~3, 5, 7, and 9,[69] respectively, the preferential photodegradation of oligomers is expected to shift the ⟨DBE⟩ to lower values. As discussed above, the dilution of the same SOA sample can also result in a decrease in ⟨DBE⟩. However, photolysis is not expected to significantly reduce the overall mass concentration in the solution. Although small photolysis products may leave the solution by evaporation they are likely to represent only a small fraction of the mass of the dissolved organic compounds. Therefore, we do not believe that the dilution effects contribute significantly to the observed ⟨DBE⟩ reduction.

Closer examination of the mass spectra reveals the appearance/disappearance of a number of peaks during photolysis as well as significant changes in peak abundances.

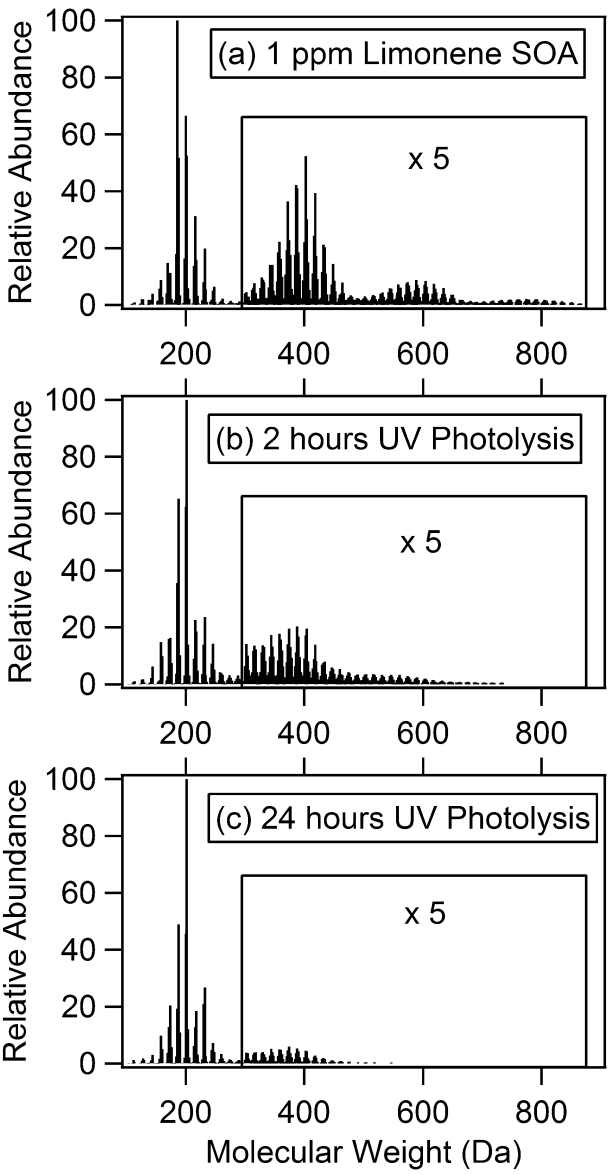

Fig. 2 Representative ESI (−) mass spectra of 1 ppm limonene SOA collected with PILS: (a) before photolysis; (b) after 2 h of photolysis, and (c) after 24 h of photolysis. The corresponding ESI (+) spectra are included in the SI section† in Fig. S3. All peaks are normalized to the most abundant peak in each mass spectrum. The observed m/z values have been converted to molecular weights of the neutral compounds.

Although peak intensities in the ESI mass spectra of mixtures are not directly proportional to the concentrations,[89] the expectation is that peaks corresponding to photodegradable compounds should decrease in abundance or even disappear, whereas peaks corresponding to stable photolysis products should increase. It is therefore instructive to group SOA compounds based on the observed changes (α_i) to their abundance (x_i) in the mass spectrum:

$$\alpha_i = \frac{x_i^{\text{after photolysis}}}{x_i^{\text{before photolysis}}} \quad (6)$$

Values of α are then grouped into five categories: new compounds produced from photolysis (α = "infinity"); increased relative

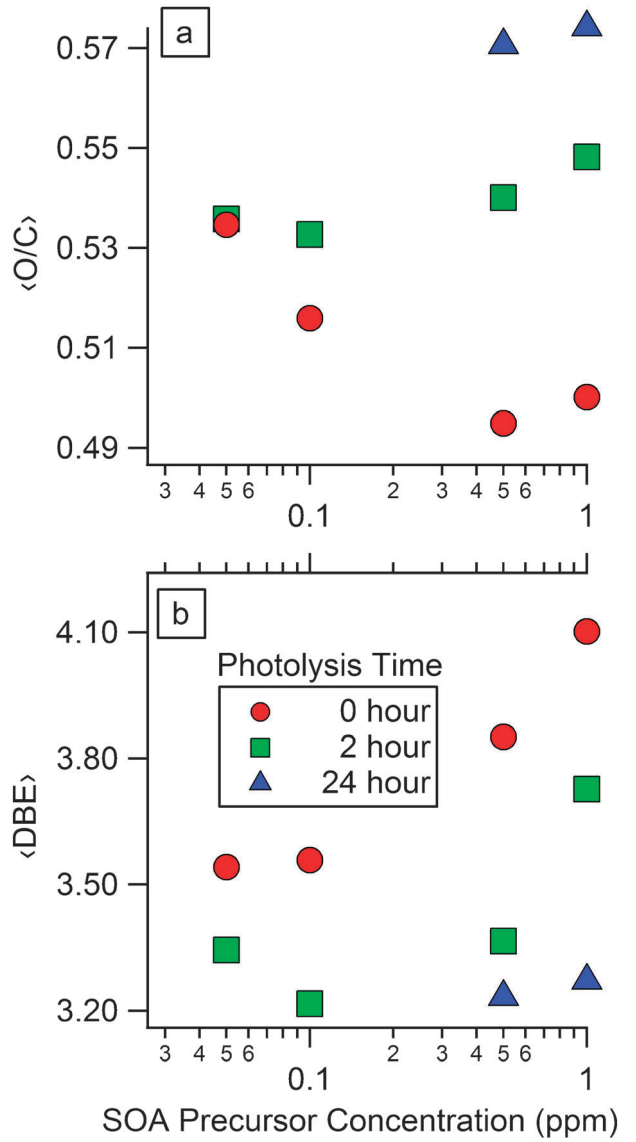

Fig. 3 Average values of (a) O/C and (b) DBE calculated from ESI (−) mass spectra obtained at different precursor concentrations and aqueous SOA extract photolysis times. The 24 h photolysis experiments were only conducted with the 0.5 ppm and 1 ppm data sets. The average O/C increases and DBE decreases with the photolysis time, especially at larger SOA loadings.

abundance from photolysis ($\alpha > 2$); no significant change from photolysis ($2 > \alpha > 0.5$); decreased relative abundance from photolysis ($\alpha < 0.5$); and compounds obliterated by photolysis ($\alpha = 0$). The average O/C, H/C, DBE value and #C were then calculated for each of these five categories, along with the percentage of the total abundance for each group. Table 2 lists these values calculated from 2 h and 24 h of photolysis for 1 ppm limonene SOA in ESI (+) and (−) modes. The new photochemically formed compounds have higher ⟨O/C⟩ values compared to the other types of compounds but are of relatively low abundance. Compounds that increased in relative abundance ($\alpha > 2$) also have higher than average ⟨O/C⟩ and represent ~25% of the total signal. Conversely, compounds that are detected with decreased relative abundances ($0 < \alpha < 0.5$) have lower ⟨O/C⟩, and contribute to ~10% of the total signal. Lastly, compounds that have been completely decomposed during photolysis (~10% of the total signal) have relatively low ⟨O/C⟩ and the highest values of ⟨DBE⟩ compared to the other groups. The trends in the ⟨H/C⟩ values are anti-correlated with the trends in the ⟨O/C⟩ values, *i.e.*, compounds with high ⟨H/C⟩ are more likely to be removed by photolysis, and low ⟨H/C⟩ compounds are more likely to be the products.

The average O/C value of the *monomeric* compounds that are decomposed by photolysis is low (ESI (+) ~ 0.34; ESI (−) ~ 0.45) compared to that of the entire monomeric region (ESI (+) ~ 0.45; ESI (−) ~ 0.57). Taken with the data from Table 2, the observed increase in the overall ⟨O/C⟩ (Fig. 3a) and decrease in the overall ⟨DBE⟩ values (Fig. 3b) can be best described as "photodegradation of low O/C monomers and high DBE oligomers of SOA with production of high O/C compounds". These results are consistent with previously reported data on aqueous photolysis of DOM samples.[48,49] HR-ESI-MS analysis of DOM before and after photolysis showed that chemical families with high DBE and low oxygen number are preferentially photolyzed, while compounds with low DBE and high oxygen content remained intact after photolysis.[49] Another study found that hydrophilic moieties were preferentially degraded from photolysis, while more hydrophobic moieties remained unaffected, or were formed.[48]

The effect of photolysis on individual functional groups was further examined using methanol reactivity analysis.[7] The subset of peaks corresponding to aldehydes is significantly reduced by the UV photolysis, sometimes to the point of complete annihilation. For example, the compound $C_{10}H_{16}O_2$, previously identified as limononaldehyde,[8] decreases from 36% to 1% relative abundance after only 2 h of photolysis, as measured in the ESI (+) mode. The peaks corresponding to compounds assigned as ketones are also reduced by UV photolysis. For example, the compound $C_9H_{14}O_4$, previously assigned to keto-limononic acid, decreases from 100% to 35% relative abundance after 2 h of photolysis, as measured in the ESI (−) mode.

Cumulative analysis of the complete set of compounds grouped by carbonyl, carboxyl, both carbonyl and carboxyl groups, or other functional group is tabulated in Table 3 (1 ppm data only). The data obtained from photolysis of 0.5, 0.1, and 0.05 ppm samples can be found in Table S4 of the SI section.† Compounds containing both carbonyl and carboxyl groups comprise the largest fraction (~70%) of the total HR-MS signal, emphasizing the multifunctional nature of the SOA constituents. Upon photolysis, this fraction decreases to ~60%, suggesting that these multifunctional compounds containing one or more carbonyl groups are dissociated. Carbonyl-only compounds (with no carboxyl group) account for a relatively small fraction (~6–8%) of the total signal. This fraction is decreased by photolysis as well, all in agreement with the UV/Vis measurements described below. The signal corresponding to compounds containing only carboxylic acid groups increased with photolysis relative to the starting solution. Finally, compounds classified in the other functional group category, increase in their relative abundance. However, part of this increase is due

Table 2 Average values of O/C, H/C, DBE, #C and percent ion current for limonene SOA compounds after 2 and 24 h of photolysis. The SOA compounds have been grouped according to the response of the corresponding peaks in the mass spectra to photolysis. The top and bottom sections of the table were calculated from ESI (−) and (+) mass spectra, respectively. Compounds with low O/C and large DBE values are photolyzed preferentially giving rise to new compounds with lower DBE and increased O/C

		2 h photolysis					24 h photolysis				
		⟨O/C⟩	⟨H/C⟩	⟨DBE⟩	⟨#C⟩	% Ion current	⟨O/C⟩	⟨H/C⟩	⟨DBE⟩	⟨#C⟩	% Ion current
ESI (−) mode	New compounds	0.68	1.44	5.11	14.0	1	0.72	1.47	4.09	10.7	1
	Increased relative abundance	0.59	1.54	3.58	11.0	23	0.65	1.45	3.46	8.9	20
	No change	0.55	1.54	3.65	11.6	64	0.57	1.55	3.07	9.2	65
	Decreased relative abundance	0.45	1.56	4.38	15.7	11	0.47	1.54	3.92	12.8	14
	Destroyed compounds[a]	0.46	1.59	7.43	31.5	5[a]	0.48	1.58	6.67	27.0	16[a]
ESI (+) mode	New compounds	0.50	1.55	3.94	11.6	1	0.54	1.54	3.21	8.4	1
	Increased relative abundance	0.48	1.56	3.03	9.0	27	0.48	1.52	2.98	8.1	53
	No change	0.42	1.60	3.29	11.3	62	0.43	1.55	3.36	10.2	37
	Decreased relative abundance	0.38	1.59	4.40	16.8	10	0.39	1.66	3.27	12.7	10
	Destroyed compounds[a]	0.41	1.57	7.00	28.8	5[a]	0.41	1.57	6.00	23.6	15[a]

[a] Percent ion current calculated from non-photolyzed mass spectra.

Table 3 Effect of photolysis on the estimated percent fraction of carbonyls and carboxyls in the 1 ppm limonene SOA extract (the concentration dependence of these fractions is provided in Table S4 of the SI section†). The fraction of HR-MS signal was calculated for each group, from the corresponding mass spectra taken before photolysis, after 2 h, and after 24 h of photolysis

ESI (−) mode	Carbonyl	Carboxyl	Both	Other	Total ion signal
No Photolysis	6.2	8.2	74.0	11.6	1.0
2 h Photolysis	5.7	12.5	62.2	19.6	1.0
24 h Photolysis	4.4	11.3	64.5	19.9	0.8
ESI (+) mode	**Carbonyl**	**Carboxyl**	**Both**	**Other**	**Total ion signal**
No Photolysis	8.1	13.9	69.3	8.7	1.0
2 h Photolysis	4.7	25.4	55.7	14.2	0.84
24 h Photolysis	3.2	19.1	58.0	19.7	0.47

to the artificial attribution of all the new compounds generated by photolysis to the ''other'' category.

In order to investigate the role of aqueous solvation on the photochemistry of limonene SOA, we have also conducted photolysis experiments on dry limonene SOA. Table 4 compares the average elemental ratios and average DBE values as measured in the (+) and (−) modes for 0.5 ppm and 1 ppm precursor concentrations photolyzed for 2 h in aqueous solution and directly on a filter. Table S5 in the SI section† (which is similar to Table 3 for the aqueous photolysis data) bins the compounds according to the ratio α of eqn (6), for the filter photolysis from 0.5 ppm and 1 ppm samples. Surprisingly, the overall trends for the filter photolysis are not substantially different from those observed in the aqueous photolysis experiments, but photolysis in aqueous solution appears to be more efficient than photolysis on a filter. For example, both the increase in ⟨O/C⟩ and decrease in ⟨DBE⟩ are smaller in magnitude on the filter. It is likely that the more viscous environment in dry particles suppresses diffusion of free radical intermediates and increases the probability of geminate recombination making the photolysis less efficient.

Effect of photolysis on the UV/Vis spectra of limonene SOA in water

Characteristic UV/Vis spectra of 1 ppm limonene SOA aqueous solutions acquired during photolysis of PILS samples are shown in Fig. 4. The response of the spectrum around 280 nm is especially interesting as it includes contributions from the $n \rightarrow \pi^*$ bands in carbonyls, with additional contributions from the $n \rightarrow \sigma^*$ bands in peroxides.[98] Furthermore, 280 nm is close to the cut-off wavelength for tropospheric photochemistry, with higher-energy radiation being effectively screened by stratospheric ozone. After only thirty minutes of photolysis the optical absorbance at 280 nm is visibly diminished, and after 24 h, most of the initial absorbance at this wavelength has disappeared. The effective photolysis lifetime measured at 280 nm absorbance was $\sim$105 min as estimated from an exponential fit to the measured absorbance (inset of Fig. 4). At lower wavelengths, there was an initial gain in absorbance between 210–240 nm followed by a decrease after 24 h of photolysis. In this wavelength range it is more difficult to attribute the change in absorbance to any particular functional group.

The efficiency of photolysis can be estimated by comparing the observed decay of the 280 nm absorbance with the excitation rate. The effective photolysis rate (J, in units of s^{-1}) of an SOA constituent is

$$J = \int_{\lambda} \sigma(\lambda)\phi(\lambda)F(\lambda)d\lambda \qquad (7)$$

where $\sigma(\lambda)$ is the effective absorption cross section in cm^2 $molecule^{-1}$, $\varphi(\lambda)$ is the effective photolysis quantum yield, $F(\lambda)$ is the radiation flux density in photons cm^2 nm^{-1}, and λ is the wavelength. The same expression with $\varphi(\lambda) = 1$ gives the excitation rate. The effective absorption cross section (base-e) can be obtained from the experimentally measured base-10 absorbance (A_{10}) as follows:

$$\sigma(\lambda) = \frac{A_{10}(\lambda) \cdot \ln(10)}{\ell \cdot C \cdot N_a \cdot 10^{-3}} \qquad (8)$$

where ℓ is the cuvette path length in cm, C is the concentration in mol L^{-1}, and N_a is Avogadro's number. The molar concentration of SOA compounds is estimated from the SMPS data (Table 1), assuming 100% PILS collection efficiency. We assume an effective molecular weight of 200 g/mol, as this is the average molecular weight of the monomer species observed

Table 4 Average values of O/C, H/C, DBE and number of carbons for SOA photolyzed in a dry state directly on a filter or in aqueous solution. The values were calculated from mass spectra taken before and after photolysis (in the filter case, the samples are extracted in H_2O and diluted with CH_3CN immediately before taking the mass spectra). The top and bottom sections of the table were calculated from ESI (−) and (+) mass spectra, respectively

SOA precursor concentration (ppm)/Medium		0.50/Solution	0.50/Filter	1.00/Solution	1.00/Filter
ESI (−) mode	⟨O/C⟩ Before UV	0.49	0.50	0.50	0.50
	⟨O/C⟩ 2 h UV	0.54	0.52	0.55	0.53
	⟨H/C⟩ Before UV	1.55	1.54	1.55	1.54
	⟨H/C⟩ 2 h UV	1.55	1.54	1.54	1.53
	⟨DBE⟩ Before UV	3.85	3.93	4.10	3.88
	⟨DBE⟩ 2 h UV	3.37	3.94	3.73	4.22
	⟨#C⟩ Before UV	12.89	12.87	14.08	12.61
	⟨#C⟩ 2 h UV	10.63	12.76	11.93	13.73
ESI (+) mode	⟨O/C⟩ Before UV	0.39	0.38	0.39	0.40
	⟨O/C⟩ 2 h UV	0.43	0.43	0.44	0.43
	⟨H/C⟩ Before UV	1.59	1.57	1.59	1.58
	⟨H/C⟩ 2 h UV	1.61	1.61	1.59	1.59
	⟨DBE⟩ Before UV	3.69	4.10	3.80	4.18
	⟨DBE⟩ 2 h UV	3.11	3.60	3.35	3.89
	⟨#C⟩ Before UV	12.94	14.41	13.57	15.29
	⟨#C⟩ 2 h UV	10.62	10.53	11.23	13.97

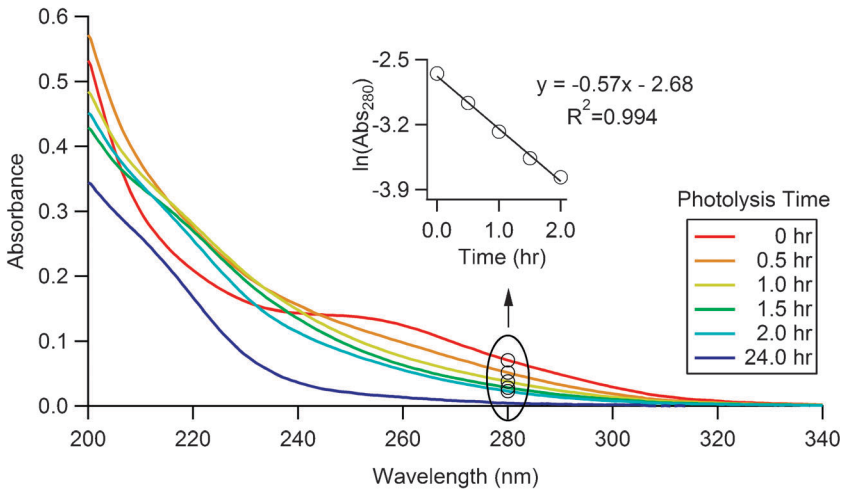

Fig. 4 UV/Vis spectra taken during photolysis of 1 ppm limonene SOA sample collected using PILS. Spectra were obtained every thirty minutes during the first two hours of photolysis and again after 24 h of photolysis. The inset shows the natural log of absorbance at 280 nm *versus* photolysis time. The lifetime with respect to photolysis is about 1.75 h.

in the ESI mass spectra. The integrated radiation flux can be related to the total power measured at the position of the photolysis cell.

$$\text{Measured Power} = S\int_{\lambda} F(\lambda)\frac{hc}{\lambda}d\lambda \qquad (9)$$

where S is equal to the beam surface area, h is Planck's constant, and c is the speed of light. The shape of the wavelength dependence of $F(\lambda)$ is obtained from explicit measurements with an Ocean Optics spectrometer.

Using eqn (7)–(9), we estimate an excitation rate of 0.0053 s^{-1} for the sample shown in Fig. 4. This rate is significantly larger than the observed rate of disappearance of the $n \rightarrow \pi^*$ carbonyl band (0.00016 s^{-1} from Fig. 4). The wavelength-integrated photolysis quantum yield (φ) can be estimated as the ratio of these two rates. The resulting value of $\varphi = 0.03$, compares favorably with known quantum yields for carbonyl photolysis in liquid hydrocarbons (0.005–0.02).[99] The low values are indicative of solution-phase carbonyl photolysis, with quantum yields reduced relative to the gas-phase.[100]

Although other compounds, such as peroxides, undergo direct photolysis in this wavelength range, both the shape of the absorption spectrum and the order of magnitude of the estimated photolysis quantum yield strongly suggest that carbonyl photochemistry plays a very important role in photolytic processing of SOA aqueous solutions. This conclusion is consistent with previous studies, where significant photochemical transformation of aqueous solutions of pyruvic acid and glycolaldehyde was observed upon exposure to actinic UV radiation.[44,45,52,56,57]

Effect of photolysis on the pH and peroxide content of limonene SOA in water

To further confine the effects of photolysis on chemical composition, pH and peroxide measurements of the SOA

extracts were performed before and after photolysis. The pH measurements provide indirect information about the total concentration of acidic species in SOA, and the peroxide test quantifies the total amount of water-soluble organic peroxides and hydrogen peroxide. As limonene SOA is water-soluble at the concentrations used in this work,[70] the peroxide test should measure the total peroxide content in the solutions.

Fig. 5 plots the observed pH (a) and peroxide concentration (b) *vs*. the SOA precursor concentrations: before, after 2 h, and after 24 h of photolysis. Before photolysis, the measured pH decreases and peroxide concentration increases with the SOA precursor concentrations. These changes are expected because the mass of SOA extracted in water increases at higher precursor concentrations (Table 1). It is therefore more informative to compare the molar amounts of hydronium ion and peroxides normalized with respect to the mass of dissolved SOA (in the units of moles per mg of dissolved SOA) as done in Fig. 5c. The normalized amounts ($\sim 10^{-7}$ mol mg^{-1}) do not depend on SOA loading within experimental uncertainties.

With the assumed average molecular weight of 200 g/mol for SOA compounds, our measurements suggest that there is one peroxide group per 50 SOA molecules ($\sim$2%). This number is significantly lower compared to measurements by Dochtery *et al*. for α-pinene ($\sim$47%) and β-pinene ($\sim$85%).[85] The reasons for this discrepancy are not entirely clear but they may have to do with the differences in the experimental conditions. For example, our measurements were for the water-soluble fraction only, while Dochtery *et al*. measured the organic-soluble fraction. The reactant concentrations were higher in the Dochtery *et al*. study, and they used a scavenger that suppressed oxidation by OH. Our results are in much better agreement with the recent measurements of reactive oxygen species (ROS) in limonene SOA by Chen *et al*., who reported ROS yields in fresh limonene SOA of the order of 1–2%.[101]

Estimating the fraction of carboxyl groups from the pH measurements is less straightforward, as we do not account for the effect of the dissolved atmospheric CO_2 (photolysis and pH measurements were done in room air) and incomplete ionization of acids. pK_a values for the common acids found in biogenic SOA are in the 3–5 range (*e.g*., pK_a = 4.6 for pinonic acid) and not all of these carboxylic acids are expected to ionize in solution at pH = 4–6. In addition, compounds other than carboxylic acids can have pK_a values in this range, for example, enols such as ascorbic acid, have a pK_a value of $\sim$4. Therefore, the proton concentration derived from pH measurements underestimates the concentration of acidic species, perhaps by as much as an order of magnitude. However, in photolysis experiments, pH can still be used as a metric for the relative amounts of acidic species in SOA.

A reproducible reduction in pH was observed for all photolyzed SOA extracts (Fig. 5). The carboxylic acid group by itself is not photochemically active at tropospherically relevant wavelengths.[102] However, it can participate in photochemistry if positioned next to a photochemically active group. For example, pyruvic acid ($CH_3C(O)COOH$) undergoes decarboxylation and photopolymerization quite readily when irradiated at 320 nm.[52] Many carboxylic acids in limonene SOA are multifunctional compounds, and some of

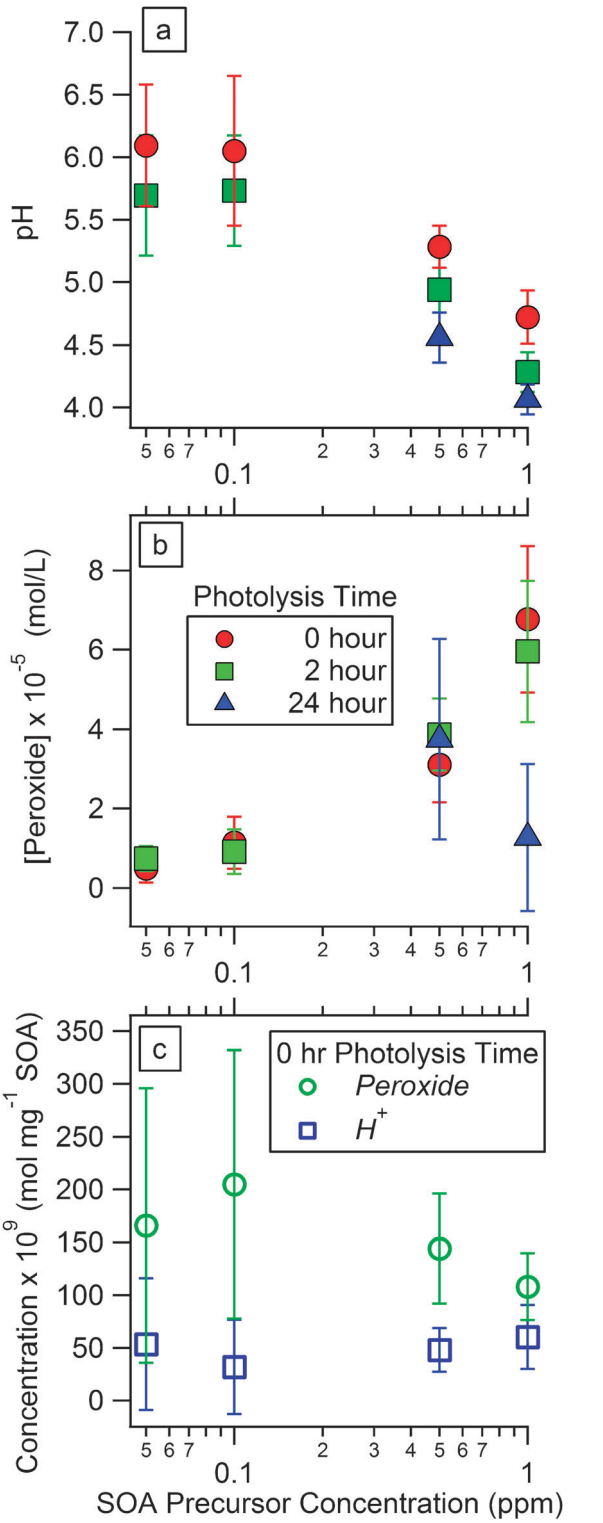

Fig. 5 (a) Absolute pH values, and (b) peroxide concentrations measured in PILS samples of limonene SOA with varying precursor concentrations and photolysis times. (c) Normalized concentrations (in units of mol per mg of the dissolved SOA mass) of H^+ ion and peroxides measured in collected PILS vials from limonene SOA before photolysis. The mass of SOA collected was estimated using values in Table 1 and assuming a 100% PILS collection efficiency.

them may undergo similar photochemical processes. However, the decrease in pH suggests that production of carboxylic acids and other acidic compounds as end products of photolysis outweighs their decomposition. Photochemical production of carboxylic acids has been observed in aqueous solutions of DOM. For example, a study on soil derived humic substances observed an increase in acidic species due to photolysis in the presence of dissolved oxygen.[46] Another study reported low-molecular weight acid (formic, acetic, pyruvic, oxalic, malonic and succinic acids) formation from photolysis of DOM.[48] It appears that similar photochemical processes occur in SOA and DOM extracts with respect to the carboxylic acid production.

Based on the efficient photodegradation of carbonyls described in the previous section, we expected to find a similarly large reduction in the peroxide content in the photolyzed SOA extracts. While there is no experimental information on the photodissociation quantum yields of large organic peroxides in aqueous solutions, the yields are likely to be high based on comparison to the H_2O_2 and CH_3OOH aqueous photolysis.[103,104] Using absorption cross sections and photolysis quantum yields for H_2O_2 or CH_3OOH in eqn (7)–(9), we estimated that peroxides should undergo photodegradation as fast if not faster than carbonyls. However, according to Fig. 5, the peroxide concentrations did not change after 2 h of photolysis within the measurement uncertainties. After 24 h of photolysis, the 1 ppm samples experienced a reduction in the peroxide content, while the 0.5 ppm samples had no statistically significant change (24 h photolysis experiments at the lower SOA loadings were not conducted). Based on these observations, we conclude that the secondary reactions of the primary photolysis products must generate smaller peroxides such as H_2O_2. Indeed, photochemical production of H_2O_2 has been observed from cloudwater[43,59,60] and DOM[51] in aqueous solution. As the peroxide test employed in our analysis does not distinguish between water-soluble organic peroxides and H_2O_2,[85] the combined result of photodissociation of organic peroxides and formation of H_2O_2 would result in no net change to the observed peroxide content.

Discussion

Possible mechanisms of photolysis

Because SOA represents a very complex mixture of hundreds of organic compounds, it is unrealistic to determine a detailed mechanism of the photolytic processing of its aqueous extract. However, one can draw general conclusions about the behavior of different functional groups based on the examination of mass-spectrometric, spectroscopic, pH, and peroxide content results described in the previous sections. The goal of the following discussion is to rationalize the observed photodegradation of carbonyls (Fig. 4 and Table 3), cycling of peroxides (Fig. 5b), and photoproduction of acidic species (Fig. 5a) during photolysis.

Broadly speaking, there are two mechanisms for the photolytic processing occurring in the SOA extracts: direct photodissociation and secondary reactions with free radicals formed by the direct processes. Examples of the direct processes are $n \rightarrow \pi^*$ Norrish type-I and -II splitting of carbonyls,[105–107] and $n \rightarrow \sigma^*$ photolysis of peroxides. The observed reduction in carbonyl functional groups during photolysis is consistent with the direct photodissociation occurring in the solution. However, the fact that the total amount of peroxides does not change significantly during photolysis suggests that secondary reactions must also be taking place, and that these reactions generate peroxides and carboxylic acids as products.

Photolysis of simple organic hydroperoxides CH_3OOH and C_2H_5OOH in water has been studied extensively.[104] The primary photolysis of these peroxides results in formation of an alkoxy radical and hydroxyl radical, *e.g.*:

$$C_2H_5OOH + h\nu \rightarrow C_2H_5O^{\bullet} + HO^{\bullet} \qquad (R1)$$

Photolysis of more complex organic peroxides has not been investigated in detail but most of them likely break in a similar way *via* fission of the O–O bond:

$$ROOR' + h\nu \rightarrow RO^{\bullet} + R'O^{\bullet} \qquad (R2)$$

It has been suggested and confirmed by experiments that the alkoxy radicals isomerize in water into hydroxyalkyl radicals, which can then add oxygen to form hydroxyperoxy radicals.[104]

$$CH_3O^{\bullet} \rightarrow HOCH_2^{\bullet} \ (+O_2) \rightarrow HOCH_2OO^{\bullet} \qquad (R3)$$

Additional peroxy radicals can also be produced by direct Norrish type-I photolysis of carbonyls in the presence of dissolved oxygen:

$$R'C(O)R + h\nu \rightarrow R'C(O)^{\bullet} + R^{\bullet} \ (+O_2) \rightarrow R'C(O)OO^{\bullet} + ROO^{\bullet} \qquad (R4)$$

Norrish type-I splitting of carbonyls is the predominant path for small (C_1–C_5) carbonyls.[105–107] Norrish type-II splitting dominates in larger carbonyls with accessible hydrogen atoms in the γ-position relative to the carbonyl group. Photolysis products resulting from the Norrish type-II channel are olefins and smaller aldehydes or ketones,[100] which can then be photolyzed further by the Norrish type-I mechanism.

Hydroxyl radicals generated from the photolysis of organic hydroperoxides (R1) will react with *all* stable organic molecules present in the extract, including the hydrated aldehydes. In fact, OH oxidation has been shown to be a primary loss mechanism for small aldehydes in aqueous solutions, with carboxylic acids formed as the end products.[108–110]

The peroxy radicals, including the hydroxy substituted ones formed in (R3), are relatively stable in solution. Their primary fate is self-reaction or reaction with HO_2 radicals, which can form a number of products including, organic hydroperoxides, and aldehydes.[111] Some of the peroxy radical self-reactions will go through tetroxide intermediates, which are highly unstable and break to form carboxylic acids and hydrogen peroxide in solution:[104,112]

$$ROO^{\bullet} + R'OO^{\bullet} \rightarrow [ROOOOR'] \rightarrow \text{acids} + \text{peroxides} + \text{other products} \qquad (R5)$$

As such processes involve two free radicals, their rate should increase quadratically with the concentration of the primary absorbers. This may contribute to the faster photolytic processing of the more concentrated SOA solutions.

Atmospheric implications

We have demonstrated that the molecular composition of limonene SOA undergoes extensive changes when exposed to radiation in the tropospherically relevant region of the solar spectrum (300–400 nm). More specifically, the processed aerosol is depleted in carbonyl compounds, depleted in oligomeric compounds, and enriched in acidic compounds. Although this photolytic processing can take place in dry SOA particles it appears to be more efficient when SOA is dissolved in an aqueous solution such as cloud or fog droplets. This makes direct photolytic processing a potentially important mechanism of SOA aging in humid air.

The photolytic processing of SOA increases the average O/C ratio for the aerosol constituents, and may help account for the discrepancy between lower $\langle O/C \rangle$ values measured in chamber studies and higher $\langle O/C \rangle$ values measured in the field.[113] For example, AMS measurements[114] reported $\langle O/C \rangle$ ratios of $\sim$0.7 for low-volatility OA and $\sim$0.4 for semi-volatile OA for a wide range of ambient aerosols.[115] The SOA generated by oxidation of monoterpenes generally falls into the semi-volatile OA category with $\langle O/C \rangle$ of 0.3–0.5. Extensive photolytic processing, in cloud water and in the dry state, has the potential to enrich SOA with higher O/C compounds, and gradually shift it the low volatility OA category.

The preferred photodegradation of the oligomeric compounds may contribute to the scarcity of their observations in field studies as opposed to the laboratory investigations in smog chambers.[116] The main reason oligomers are harder to observe in the field is the much lower organic loadings compared to the chamber studies but aqueous photolysis may also contribute. While actinic radiation is often present, the high level of humidity necessary to make aqueous dissolved SOA droplets is rarely achieved in smog chambers. Unlike the smog chambers, the oligomeric compounds formed in ambient aerosols have a higher probability of photodegradation through aqueous photolytic processing before the particles (or droplets) are collected.

The optical properties of the aerosol are also affected by the photolysis. Specifically, the near-UV absorbance of limonene SOA in the carbonyl $n \rightarrow \pi^*$ absorption band is reduced significantly. The reduction in the UV absorbance suggests that photobleached SOA absorb UV radiation to a smaller extent than freshly formed SOA do. This may have implications for surface UV flux in areas characterized by significant organic air pollution.

From the perspectives of SOA aging, it is instructive to estimate the time scale of the photolytic processing and contrast it to other organic aerosol aging mechanisms, such as heterogeneous oxidation by OH. The photolytic lifetime of carbonyl compounds dissolved in cloud water can be calculated from eqn (7) using the experimentally measured absorption cross section of limonene SOA in water, the estimated quantum yield ($\sim$0.03), and the solar actinic flux measured between 290 and 500 nm.[102] At a solar zenith angle (SZA) of 10°, typical for Southern California in the summer, the resulting photolysis lifetime is $\sim$5 h. At SZA of 60°, typical of Chicago, Illinois in the winter, the lifetime increases to $\sim$9 h. We note that significant changes to ambient organic aerosol composition are known to occur on comparable time scales but they are usually attributed to heterogeneous and gas-phase OH oxidation rather than direct photolysis.[114] Given that organic particles spend days in the air in a dry state and hours in a dissolved state, photolytic processing must be an important mechanism of aging, which competes with the OH-driven chemistry. Whether the oxidation by OH or photolytic processing of aerosol is more important will depend on specific atmospheric conditions (SZA, relative humidity, cloudiness, *etc.*).

Acknowledgements

The UCI group gratefully acknowledges support by the NSF grants ATM-0831518 and CHE-0909227. A.P.B acknowledges support provided by the DOE Global Change Education Program. The PNNL group acknowledges support from the intramural research and development program of the W. R. Wiley Environmental Molecular Sciences Laboratory (EMSL). EMSL is a national scientific user facility located at PNNL, and sponsored by the Office of Biological and Environmental Research of the US PNNL is operated for US DOE by Battelle Memorial Institute under Contract No. DE-AC06-76RL0 1830.

References

1 A. Guenther, C. N. Hewitt, D. Erickson, R. Fall, C. Geron, T. Graedel, P. Harley, L. Klinger, M. Lerdau, W. A. McKay, T. Pierce, B. Scholes, R. Steinbrecher, R. Tallamraju, J. Taylor and P. Zimmerman, *J. Geophys. Res.*, 1995, **100**, 8873–8892, DOI: 10.1029/94JD02950.
2 C. Geron, R. Rasmussen, R. R. Arnts and A. Guenther, *Atmos. Environ.*, 2000, **34**, 1761–1781.
3 R. J. Griffin, D. R. C. III, R. C. Flagan and J. H. Seinfeld, *J. Geophys. Res.*, 1999, **104**, 3555–3567, DOI: 10.1029/1998JD100049.
4 T. Hoffmann, J. R. Odum, F. Bowman, D. Collins, D. Klockow, R. C. Flagan and J. H. Seinfeld, *J. Atmos. Chem.*, 1997, **26**, 189–222.
5 J. Zhang, K. E. H. Hartz, S. N. Pandis and N. M. Donahue, *J. Phys. Chem. A*, 2006, **110**, 11053–11063.
6 T. Wainman, J. F. Zhang, C. J. Weschler and P. J. Lioy, *Environ. Health Perspect.*, 2000, **108**, 1139–1145.
7 A. P. Bateman, M. L. Walser, Y. Desyaterik, J. Laskin, A. Laskin and S. A. Nizkorodov, *Environ. Sci. Technol.*, 2008, **42**, 7341–7346.
8 M. L. Walser, Y. Desyaterik, J. Laskin, A. Laskin and S. A. Nizkorodov, *Phys. Chem. Chem. Phys.*, 2008, **10**, 1009–1022.
9 P. Wolkoff, P. A. Clausen, C. K. Wilkins and G. D. Nielsen, *Indoor Air*, 2000, **10**, 82–91.
10 E. R. Graber and Y. Rudich, *Atmos. Chem. Phys.*, 2006, **6**, 729–753.
11 X. Pan, J. S. Underwood, J. H. Xing, S. A. Mang and S. A. Nizkorodov, *Atmos. Chem. Phys.*, 2009, **9**, 3851–3865.
12 S. A. Mang, D. K. Henricksen, A. P. Bateman, M. P. S. Andersen, D. R. Blake and S. A. Nizkorodov, *J. Phys. Chem. A*, 2008, **112**, 8337–8344.

13 M. L. Walser, J. Park, A. L. Gomez, A. R. Russell and S. A. Nizkorodov, *J. Phys. Chem. A*, 2007, **111**, 1907–1913.
14 L. N. Hawkins and L. M. Russell, *Atmos. Environ.*, 2010, **44**, 4142–4154.
15 V. Varutbangkul, F. J. Brechtel, R. Bahreini, N. L. Ng, M. D. Keywood, J. H. Kroll, R. C. Flagan, J. H. Seinfeld, A. Lee and A. H. Goldstein, *Atmos. Chem. Phys.*, 2006, **6**, 2367–2388.
16 J. Duplissy, M. Gysel, M. R. Alfarra, J. Dommen, A. Metzger, A. S. H. Prevot, E. Weingartner, A. Laaksonen, T. Raatikainen, N. Good, S. F. Turner, G. McFiggans and U. Baltensperger, *Geophys. Res. Lett.*, 2008, **35**, L03818, DOI: 10.1029/2007GL031075.
17 K. E. H. Hartz, T. Rosenoern, S. R. Ferchak, T. M. Raymond, M. Bilde, N. M. Donahue and S. N. Pandis, *J. Geophys. Res.*, 2005, **110**, D14208, DOI: 10.1029/2004JD005754.
18 E. Dinar, I. Taraniuk, E. R. Graber, T. Anttila, T. F. Mentel and Y. Rudich, *J. Geophys. Res.*, 2007, **112**, D05211, DOI: 10.1029/2006jd007442.
19 T. M. VanReken, N. L. Ng, R. C. Flagan and J. H. Seinfeld, *J. Geophys. Res.*, 2005, **110**, D07206, DOI: 10.1029/2004JD005465.
20 K. E. Altieri, B. J. Turpin and S. P. Seitzinger, *Atmos. Chem. Phys.*, 2009, **9**, 2533–2542.
21 J. D. Willey, R. J. Kieber, M. S. Eyman and G. B. Avery, *Global Biogeochem. Cycles*, 2000, **14**, 139–148.
22 P. A. Raymond, *Geophys. Res. Lett.*, 2005, **32**, L14402, DOI: 10.1029/2005gl022879.
23 K. Kawamura, S. Steinberg and I. R. Kaplan, *Atmos. Environ.*, 1996, **30**, 1035–1052.
24 G. B. Avery, R. J. Kieber, M. Witt and J. D. Willey, *Atmos. Environ.*, 2006, **40**, 1683–1693.
25 R. M. Pena, S. Garcia, C. Herrero, M. Losada, A. Vazquez and T. Lucas, *Atmos. Environ.*, 2002, **36**, 5277–5288.
26 M. O. Andreae, R. W. Talbot, T. W. Andreae and R. C. Harriss, *J. Geophys. Res.*, 1988, **93**, 1616–1624.
27 J. E. Birdwell and K. T. Valsaraj, *Atmos. Environ.*, 2010, **44**, 3246–3253.
28 L. R. Mazzoleni, B. M. Ehrmann, X. H. Shen, A. G. Marshall and J. L. Collett, *Environ. Sci. Technol.*, 2010, **44**, 3690–3697.
29 S. Raja, R. Raghunathan, R. R. Kommalapati, X. H. Shen, J. L. Collett and K. T. Valsaraj, *Atmos. Environ.*, 2009, **43**, 4214–4222.
30 J. L. Collett, P. Herckes, S. Youngster and T. Lee, *Atmos. Res.*, 2008, **87**, 232–241.
31 A. Gelencser, M. Sallai, Z. Krivacsy, G. Kiss and E. Meszaros, *Atmos. Res.*, 2000, **54**, 157–165.
32 P. Herckes, M. P. Hannigan, L. Trenary, T. Lee and J. L. Collett, *Atmos. Res.*, 2002, **64**, 99–108.
33 P. Herckes, J. A. Leenheer and J. L. Collett, *Environ. Sci. Technol.*, 2007, **41**, 393–399, DOI: 10.1021/es06076988.
34 Q. Zhang and C. Anastasio, *Atmos. Environ.*, 2001, **35**, 5629–5643.
35 M. C. Facchini, S. Decesari, M. Mircea, S. Fuzzi and G. Loglio, *Atmos. Environ.*, 2000, **34**, 4853–4857.
36 S. Decesari, M. C. Facchini, S. Fuzzi and E. Tagliavini, *J. Geophys. Res.*, 2000, **105**, 1481–1489.
37 G. Kiss, B. Varga, A. Gelencser, Z. Krivacsy, A. Molnar, T. Alsberg, L. Persson, H. C. Hansson and M. C. Facchini, *Atmos. Environ.*, 2001, **35**, 2193–2200.
38 S. Fuzzi, M. C. Facchini, S. Decesari, E. Matta and M. Mircea, *Atmos. Res.*, 2002, **64**, 89–98.
39 R. Hitzenberger, A. Berner, A. Kasper-Giebl, M. Loflund and H. Puxbaum, *J. Geophys. Res.*, 2002, **107**, 4752, DOI: 10.1029/2002JD002506.
40 A. Cappiello, E. De Simoni, C. Fiorucci, F. Mangani, P. Palma, H. Trufelli, S. Decesari, M. C. Facchini and S. Fuzzi, *Environ. Sci. Technol.*, 2003, **37**, 1229–1240.
41 S. Enami, M. R. Hoffmann and A. J. Colussi, *J. Phys. Chem. Lett.*, 2010, **1**, 2374–2379.
42 B. C. Faust, *Environ. Sci. Technol.*, 1994, **28**, A217–A222.
43 C. Anastasio, B. C. Faust and J. M. Allen, *J. Geophys. Res.*, 1994, **99**, 8231–8248.
44 A. G. Rincon, M. I. Guzman, M. R. Hoffmann and A. J. Colussi, *J. Phys. Chem. A*, 2009, **113**, 10512–10520.
45 A. G. Rincon, M. I. Guzman, M. R. Hoffmann and A. J. Colussi, *J. Phys. Chem. Lett.*, 2010, **1**, 368–373.
46 P. Schmitt-Kopplin, N. Hertkorn, H.-R. Schulten and A. Kettrup, *Environ. Sci. Technol.*, 1998, **32**, 2531–2541.
47 R. Del Vecchio and N. V. Blough, *Mar. Chem.*, 2002, **78**, 231–253.
48 T. Brinkmann, P. Horsch, D. Sartorius and F. H. Frimmel, *Environ. Sci. Technol.*, 2003, **37**, 4190–4198.
49 E. B. Kujawinski, R. Del Vecchio, N. V. Blough, G. C. Klein and A. G. Marshall, *Mar. Chem.*, 2004, **92**, 23–37.
50 M. Gonsior, B. M. Peake, W. T. Cooper, D. Podgorski, J. D'Anrilli and W. J. Cooper, *Environ. Sci. Technol.*, 2009, **43**, 698–703.
51 R. M. Dalrymple, A. K. Carfagno and C. M. Sharpless, *Environ. Sci. Technol.*, 2010, **44**, 5824–5829.
52 M. I. Guzman, A. J. Colussi and M. R. Hoffmann, *J. Phys. Chem. A*, 2006, **110**, 3619–3626.
53 B. C. Faust, K. Powell, C. J. Rao and C. Anastasio, *Atmos. Environ.*, 1997, **31**, 497–510.
54 Y. B. Lim, Y. Tan, M. J. Perri, S. P. Seitzinger and B. J. Turpin, *Atmos. Chem. Phys.*, 2010, **10**, 10521–10539.
55 K. E. Altieri, S. P. Seitzinger, A. G. Carlton, B. J. Turpin, G. C. Klein and A. G. Marshall, *Atmos. Environ.*, 2008, **42**, 1476–1490.
56 M. J. Perri, S. Seitzinger and B. J. Turpin, *Atmos. Environ.*, 2009, **43**, 1487–1497.
57 K. E. Altieri, A. G. Carlton, H. J. Lim, B. J. Turpin and S. P. Seitzinger, *Environ. Sci. Technol.*, 2006, **40**, 4956–4960.
58 A. G. Carlton, B. J. Turpin, K. E. Altieri, S. Seitzinger, A. Reff, H. J. Lim and B. Ervens, *Atmos. Environ.*, 2007, **41**, 7588–7602.
59 T. Arakaki, C. Anastasio, P. G. Shu and B. C. Faust, *Atmos. Environ.*, 1995, **29**, 1697–1703.
60 B. C. Faust, C. Anastasio, J. M. Allen and T. Arakaki, *Science*, 1993, **260**, 73–75.
61 B. Warscheid and T. Hoffmann, *Rapid Commun. Mass Spectrom.*, 2001, **15**, 2259–2272.
62 B. Warscheid and T. Hoffmann, *Rapid Commun. Mass Spectrom.*, 2002, **16**, 496–504.
63 S. Leungsakul, M. Jaoui and R. M. Kamens, *Environ. Sci. Technol.*, 2005, **39**, 9583–9594.
64 J. K. Nojgaard, A. W. Norgaard and P. Wolkoff, *Atmos. Environ.*, 2007, **41**, 8345–8354.
65 K. J. Heaton, M. A. Dreyfus, S. Wang and M. V. Johnston, *Environ. Sci. Technol.*, 2007, **41**, 6129–6136.
66 M. Glasius, M. Duane and B. R. Larsen, *J. Chromatogr., A*, 1999, **833**, 121–135.
67 M. Glasius, M. Lahaniati, A. Calogirou, D. Di Bella, N. R. Jensen, J. Hjorth, D. Kotzias and B. R. Larsen, *Environ. Sci. Technol.*, 2000, **34**, 1001–1010.
68 J. D. Hearn and G. D. Smith, *Int. J. Mass Spectrom.*, 2006, **258**, 95–103.
69 A. P. Bateman, S. A. Nizkorodov, J. Laskin and A. Laskin, *Phys. Chem. Chem. Phys.*, 2009, **11**, 7931–7942.
70 A. P. Bateman, S. A. Nizkorodov, J. Laskin and A. Laskin, *Anal. Chem.*, 2010, **82**, 8010–8016.
71 A. Reinhardt, C. Emmenegger, B. Gerrits, C. Panse, J. Dommen, U. Baltensperger, R. Zenobi and M. Kalberer, *Anal. Chem.*, 2007, **79**, 4074–4082.
72 T. B. Nguyen, A. P. Bateman, D. L. Bones, S. A. Nizkorodov, J. Laskin and A. Laskin, *Atmos. Environ.*, 2010, **44**, 1032–1042.
73 A. Laskin, J. S. Smith and J. Laskin, *Environ. Sci. Technol.*, 2009, **43**, 3764–3771.
74 J. S. Smith, A. Laskin and J. Laskin, *Anal. Chem.*, 2009, **81**, 1512–1521.
75 A. S. Wozniak, J. E. Bauer, R. L. Sleighter, R. M. Dickhut and P. G. Hatcher, *Atmos. Chem. Phys.*, 2008, **8**, 5099–5111.
76 K. J. Heaton, R. L. Sleighter, P. G. Hatcher, W. A. Hall and M. V. Johnston, *Environ. Sci. Technol.*, 2009, **43**, 7797–7802.
77 P. Schmitt-Kopplin, A. Gelencser, E. Dabek-Zlotorzynska, G. Kiss, N. Hertkorn, M. Harir, Y. Hong and I. Gebefugi, *Anal. Chem.*, 2010, **82**, 8017–8026.
78 B. P. Koch, M. R. Witt, R. Engbrodt, T. Dittmar and G. Kattner, *Geochim. Cosmochim. Acta*, 2005, **69**, 3299–3308.
79 W. C. Hockaday, A. M. Grannas, S. Kim and P. G. Hatcher, *Org. Geochem.*, 2006, **37**, 501–510.

80 R. L. Sleighter and P. G. Hatcher, *Mar. Chem.*, 2008, **110**, 140–152.
81 E. B. Kujawinski, K. Longnecker, N. V. Blough, R. Del Vecchio, L. Finlay, J. B. Kitner and S. J. Giovannoni, *Geochim. Cosmochim. Acta*, 2009, **73**, 4384–4399.
82 R. L. Sleighter, Z. F. Lie, J. H. Xue and P. G. Hatcher, *Environ. Sci. Technol.*, 2010, **44**, 7576–7582.
83 F. Herrmann, R. Winterhalter, G. K. Moortgat and J. Williams, *Atmos. Environ.*, 2010, **44**, 3458–3464.
84 A. Sorooshian, F. J. Brechtel, Y. L. Ma, R. J. Weber, A. Corless, R. C. Flagan and J. H. Seinfeld, *Aerosol Sci. Technol.*, 2006, **40**, 396–409.
85 K. S. Docherty, W. Wu, Y. B. Lim and P. J. Ziemann, *Environ. Sci. Technol.*, 2005, **39**, 4049–4059.
86 S. A. Nizkorodov, J. Laskin and A. Laskin, *Phys. Chem. Chem. Phys.*, 2011, **13**, 3612–3629.
87 B. P. Koch and T. Dittmar, *Rapid Commun. Mass Spectrom.*, 2006, **20**, 926–932.
88 J. Meija, *Anal. Bioanal. Chem.*, 2006, **385**, 486–499.
89 N. B. Cech and C. G. Enke, *Mass Spectrom. Rev.*, 2001, **20**, 362–387.
90 P. Kebarle, *J. Mass Spectrom.*, 2000, **35**, 804–817.
91 C. G. Enke, *Anal. Chem.*, 1997, **69**, 4885–4893.
92 A. Zelenyuk, M. J. Ezell, V. Perraud, S. N. Johnson, E. A. Bruns, Y. Yu, D. Imre, M. L. Alexander and B. J. Finlayson-Pitts, *Atmos. Environ.*, 2010, **44**, 1209–1218.
93 K. Matsumoto, S. Kawai and M. Igawa, *Atmos. Environ.*, 2005, **39**, 7321–7329.
94 J. W. Munger, J. Collett, B. Daube and M. R. Hoffmann, *Atmos. Environ., Part B*, 1990, **24**, 185–205.
95 R. Volkamer, P. J. Ziemann and M. J. Molina, *Atmos. Chem. Phys.*, 2009, **9**, 1907–1928.
96 Y. Q. Gao, W. A. Hall and M. V. Johnston, *Environ. Sci. Technol.*, 2010, **44**, 7897–7902.
97 J. E. Shilling, Q. Chen, S. M. King, T. Rosenoern, J. H. Kroll, D. R. Worsnop, P. F. DeCarlo, A. C. Aiken, D. Sueper, J. L. Jimenez and S. T. Martin, *Atmos. Chem. Phys.*, 2009, **9**, 771–782.
98 S. A. Mang, M. L. Walser, X. Pan, J. H. Xing, A. P. Bateman, J. S. Underwood, A. L. Gomez, J. Park and S. A. Nizkorodov, in *Atmospheric Aerosols: Characterization, Chemistry and Modeling*, ed. K. T. Valsaraj and R. R. Kommalapati, American Chemical Society, 2009, vol. 1005, pp. 91–109.
99 G. H. Harltey and J. E. Guillet, *Macromolecules*, 1968, **1**, 413–417.
100 J. N. Pitts and J. K. S. Wan, in *The Chemistry of the Carbonyl Group*, ed. S. Patai, Interscience, Chichester, 1966, p. 823.
101 X. Chen, P. K. Hopke and W. P. L. Carter, *Environ. Sci. Technol.*, 2011, **45**, 276–282.
102 B. J. Finlayson-Pitts and J. N. Pitts, *Chemistry of the Upper and Lower Atmosphere: Theory, Experiments, and Applications*, Academic Press, San Diego, 2000.
103 L. Chu and C. Anastasio, *J. Phys. Chem. A*, 2005, **109**, 6264–6271.
104 A. Monod, E. Chevallier, R. D. Jolibois, J. F. Doussin, B. Picquet-Varrault and P. Carlier, *Atmos. Environ.*, 2007, **41**, 2412–2426.
105 R. G. W. Norrish, *Trans. Faraday Soc.*, 1934, **30**, 0103–0113.
106 W. A. Noyes, in *Photochemistry and Reaction Kinetics*, ed. P. G. Ashmore, F. S. Dainton and T. M. Sugden, Cambridge University Press, Cambridge, 1967, pp. 1–21.
107 J. N. Pitts, J. K. S. Wan and E. A. Schuck, *J. Am. Chem. Soc.*, 1964, **86**, 3606.
108 R. A. Cox, K. F. Patrick and S. A. Chant, *Environ. Sci. Technol.*, 1981, **15**, 587–592.
109 W. J. McElroy and S. J. Waygood, *J. Chem. Soc., Faraday Trans.*, 1991, **87**, 1513–1521.
110 H. Xu, P. J. Wentworth, N. W. Howell and J. A. Joens, *Spectrochim. Acta, Part A*, 1993, **49**, 1171–1178.
111 B. C. Faust and J. M. Allen, *J. Geophys. Res.*, 1992, **97**, 12913–12926.
112 A. Monod, A. Chebbi, R. Durand-Jolibois and P. Carlier, *Atmos. Environ.*, 2000, **34**, 5283–5294.
113 P. F. DeCarlo, E. J. Dunlea, J. R. Kimmel, A. C. Aiken, D. Sueper, J. Crounse, P. O. Wennberg, L. Emmons, Y. Shinozuka, A. Clarke, J. Zhou, J. Tomlinson, D. R. Collins, D. Knapp, A. J. Weinheimer, D. D. Montzka, T. Campos and J. L. Jimenez, *Atmos. Chem. Phys.*, 2008, **8**, 4027–4048.
114 J. L. Jimenez, M. R. Canagaratna, N. M. Donahue, A. S. H. Prevot, Q. Zhang, J. H. Kroll, P. F. DeCarlo, J. D. Allan, H. Coe, N. L. Ng, A. C. Aiken, K. S. Docherty, I. M. Ulbrich, A. P. Grieshop, A. L. Robinson, J. Duplissy, J. D. Smith, K. R. Wilson, V. A. Lanz, C. Hueglin, Y. L. Sun, J. Tian, A. Laaksonen, T. Raatikainen, J. Rautiainen, P. Vaattovaara, M. Ehn, M. Kulmala, J. M. Tomlinson, D. R. Collins, M. J. Cubison, E. J. Dunlea, J. A. Huffman, T. B. Onasch, M. R. Alfarra, P. I. Williams, K. Bower, Y. Kondo, J. Schneider, F. Drewnick, S. Borrmann, S. Weimer, K. Demerjian, D. Salcedo, L. Cottrell, R. Griffin, A. Takami, T. Miyoshi, S. Hatakeyama, A. Shimono, J. Y. Sun, Y. M. Zhang, K. Dzepina, J. R. Kimmel, D. Sueper, J. T. Jayne, S. C. Herndon, A. M. Trimborn, L. R. Williams, E. C. Wood, A. M. Middlebrook, C. E. Kolb, U. Baltensperger and D. R. Worsnop, *Science*, 2009, **326**, 1525–1529.
115 N. L. Ng, M. R. Canagaratna, Q. Zhang, J. L. Jimenez, J. Tian, I. M. Ulbrich, J. H. Kroll, K. S. Docherty, P. S. Chhabra, R. Bahreini, S. M. Murphy, J. H. Seinfeld, L. Hildebrandt, N. M. Donahue, P. F. DeCarlo, V. A. Lanz, A. S. H. Prevot, E. Dinar, Y. Rudich and D. R. Worsnop, *Atmos. Chem. Phys.*, 2010, **10**, 4625–4641.
116 M. Hallquist, J. C. Wenger, U. Baltensperger, Y. Rudich, D. Simpson, M. Claeys, J. Dommen, N. M. Donahue, C. George, A. H. Goldstein, J. F. Hamilton, H. Herrmann, T. Hoffmann, Y. Iinuma, M. Jang, M. E. Jenkin, J. L. Jimenez, A. Kiendler-Scharr, W. Maenhaut, G. McFiggans, T. F. Mentel, A. Monod, A. S. H. Prevot, J. H. Seinfeld, J. D. Surratt, R. Szmigielski and J. Wildt, *Atmos. Chem. Phys.*, 2009, **9**, 5155–5236.

